A Bandpass Filter With Inherent Gain Adaptation for Hearing Applications

Kofi M. Odame, *Student Member, IEEE*, David V. Anderson, *Senior Member, IEEE*, and Paul Hasler, *Senior Member, IEEE*

***Abstract*—In this paper, we propose a novel bandpass filter design that incorporates automatic gain control (AGC). The gain control in the filter reduces the performance requirements of a wideband AGC, and allows for low-power multichannel compression. The filter achieves up to 15 dB of compression on a 55-dB input dynamic range and is tunable over the audio frequency range, with microwatt power consumption and $<5\%$ harmonic distortion.**

***Index Terms*—Bandpass filter, gain control, nonlinear circuits.**

I. Signal Processing in Hearing Aids

THE majority of hearing impairment is due to sensorineural loss, which is damage to, or loss of, hair cells in the cochlea. This condition is characterized by a reduction of perceivable dynamic range (e.g., in recruitment of loudness). The goal of hearing compensation in this case, be it with a hearing aid or with a cochlear implant, is to compress the normal dynamic range of hearing to compensate for the lost ability of the cochlea to adapt to the signal level [1]–[3].

There are a variety of compression schemes that are in common use in hearing aids. For a comparative review, see [4]. In a typical analog hearing aid, signal compression is applied uniformly on the entire audio bandwidth. However, since the patient's loss of dynamic range is normally frequency dependent [5], it is more beneficial to employ multichannel compression. Available in DSP-based hearing aids, multichannel compression allows individual frequency bands to be tuned for specific dynamic ranges [6]. The disadvantage of this approach is the size, power and monetary cost of the digital processor.

We favor the form of multichannel compression that is depicted in Fig. 1, but in a low-cost *analog* aid. Conceptually, our hearing compensation scheme consists of two multiple-channel filters in cascade, $H_{\rm n}$ and $H_{\rm d}$. The filter $H_{\rm n}$ mimics the normal functioning of the cochlea. The $H_{\rm d}$ filter is designed and tuned so as to provide the inverse function of the damaged cochlea. The signal $x(t)$ is thus manipulated such that the wearer perceives the original input, $s(t)$ as it would have been processed by a healthy cochlea [7]. Sound processing schemes such as this, which attempt to capture the mechanics of a biological cochlea, are probably more efficient [8] and more robust to environmental noise [9] than other algorithms.

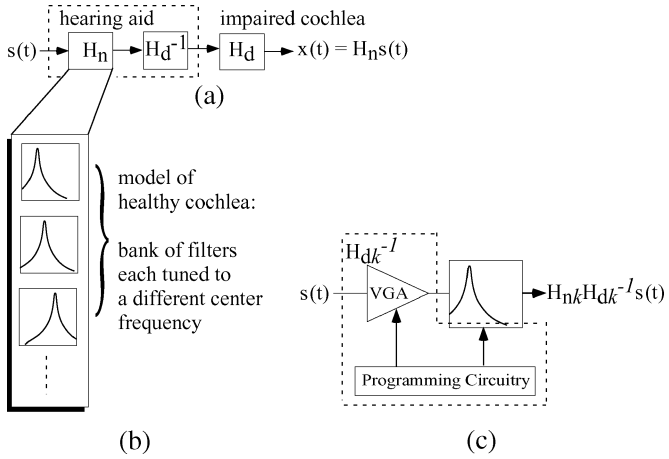

Fig. 1. Multichannel compression hearing aid. (a) The damaged cochlea is modeled as a filter $H_{\rm d}$ and the healthy cochlea is modeled as a filter $H_{\rm n}$. The hearing aid is formed from the cascade of $H_{\rm n}$ and the inverse of $H_{\rm d}$. (b) The $H_{\rm n}$ block is a bank of nonlinear bandpass filters that performs a frequency analysis of the input signal. (c) In practice, the $H_{\rm d}$ filter reduces to parameter control of each channel in the $H_{\rm n}$ filter. For the k'th channel in $H_{\rm n}$, there is a corresponding set of parameters that constitute $H_{\rm d}k$. VGA stands for variable gain amplifier, which is optional, but if present, can be used to set the knee point of the compression in terms of input amplitude (the compression scheme that we present in this paper is akin to output automatic gain control [4], [10], which defines the knee point in terms of output amplitude).

Fig. 1(b) shows that each channel of $H_{\rm n}$ contains a bandpass filter. The $H_{\rm d}$ portion of the hearing aid reduces to parameter settings for the bank of bandpass filters [see Fig. 1(c)]. This paper focuses on a suitable bandpass filter, which mimics pertinent local functionality of the cochlea's basilar membrane. The main challenge of the design is to keep power and area costs low enough for the filter to be of practical use in a portable hearing device. We will describe a nonlinear analog circuit approach that meets this challenge.

The paper is organized as follows. Section II examines at a high level the issues that our particular mode of compression would imply for speech perception. Section III is a detailed description of the filter architecture. The detail in Section IV is at an even finer level, addressing the design of specific circuit blocks in the filter. Section V provides some analysis of the filter's behavior. Finally, we present experimental results in Section VI and discuss the relevance of our novel filter to an actual hearing aid design in Section VII.

Manuscript received October 4, 2006; revised March 13, 2007 and July 20, 2007. This paper was recommended by Associate Editor A. van Schaik.

The authors are with the School of Electrical and Computer Engineering, Georgia Institute of Technology, Atlanta, GA 30332-0760 USA (e-mail: odame@ ece.gatech.edu).

Digital Object Identifier 10.1109/TCSI.2008.916553

II. Implications for Speech Perception

Compression in hearing aids can be the source of significant distortion or artifacts. For this reason, recent research [11] suggests that the best way to use compression is as an automatic gain control (AGC) that adapts slowly except as required to suppress sudden loud noises.[1] Most likely, this is because the gain functions that are typically used are decaying exponentials that can cause noticeable harmonic distortion. These functions are usually not memoryless and they may induce phase changes in the envelope that blur the temporal characteristics of the envelope. However, the operation of our proposed circuit is somewhat different, so following is a brief analysis of the signal characteristics in the context of hearing compensation.

We represent an acoustic signal as a sum of band-limited signals indexed by k; each subband representation is further decomposed into a product of an envelope (which carries the instantaneous loudness information) and a rapidly-oscillating signal (or carrier) of nearly constant power. This signal representation can be applied to auditory analysis by making the signal subbands roughly equal in bandwidth to the critical bands in the ear [7], [12]. In particular, the acoustic signal $s(t)$ is written as

$$s(t) = \sum_k e_k(t) v_k(t) \tag{1}$$

where $v_k(t)$ is a higher frequency band-limited signal or vibration with nearly constant power; and $e_k(t)$ represents the envelope variation over time. With this representation, the loudness of the signal perceived in any particular critical band of the ear is primarily controlled by operating only on the envelope in that band.

The envelope has a well-defined bandwidth that is roughly the same as the bandwidth, f_{BW}, of $v_k(t)$. In our case, the gain is a monotonic function of the envelope and is incorporated into the bandpass filter operation so the time constant for each band is approximately $1/f_{\mathrm{BW}}$. The fact that the gain function in monotonic has the following implications (see also Fig. 2).

1) The envelope at the output of our filters $\hat{e}_k(t)$ has the same general shape as $e_k(t)$ with only a change in dynamic range.
2) The output signal is in phase with the input signal—that is, the phase of $\hat{s}_k(t)$ is the same as that of $s_k(t)$ and if they were overlaid they would line up, the only difference being in the amplitude.
3) Temporal cues are preserved because of items 1 & 2 and because $v_k(t)$ is preserved.

Note, while the gain applied to the envelope does not smear or destroy temporal cues they may be slightly diminished as their dynamic range is diminished. This is to be expected since the audible dynamic range of the listener is diminished. However, this has been shown to provide an improvement in speech reception, especially in noise [13], [14]. Note that the healthy cochlea too adapts its critical-frequency gain at a rate that is on the order of one period of the input signal [15].

[1]For such a system, the perceived distortion is minimal because the slow adaptation is not very perceptible while the fast attack may be masked by the sound that caused it.

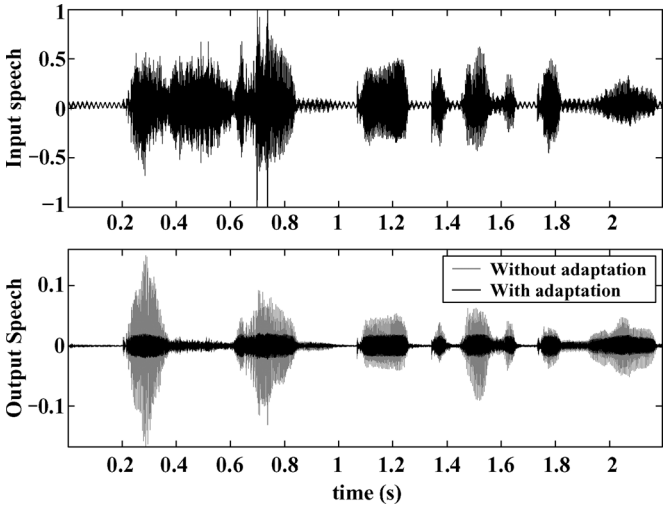

Fig. 2. Simulation results for a single band of speech processing. The upper panel is the original input speech. The lower panel is the processed speech for a single band. The black area is speech compressed with the scheme that we will describe in this paper. After compression, the general shape of the signal's envelope is maintained, but with a reduction in dynamic range.

Finally, care must be taken so that the high-Q bandpass filters do not ring too long and cause temporal smearing. This is not an issue for moderate Q values. For example, a filter with a center frequency of 1 kHz and $Q = 5$ yields 1.6 ms of ringing when measured to the 3-dB point and after 4 ms, the ringing has attenuated by over 20 dB. Thus, the ringing is much shorter than even a short speech phoneme, meaning that it is perceptually insignificant. However, we would like to have Qs that are high enough to reflect the cochlea's sharp frequency-selectivity [16]. The solution is to create high-order filters that exhibit sharp frequency selectivity without excessive ringing. While this paper focuses on a second-order filter, we can readily achieve higher orders simply by cascading multiple filters per channel.

III. Filter Description and Architecture

The cochlea can be modeled as a bank of filters that performs a frequency analysis on input signals. For small-amplitude inputs, each filter has a narrow passband around a resonant frequency. As the input signal energy in a particular bandwidth increases, the passband of the corresponding filter widens and its center frequency gain reduces. In effect, each filter exhibits a band-limited nonlinear response around its resonant frequency [17]. It is through this nonlinearity that the healthy cochlea is able to compress a wide input dynamic range into a much smaller internal one.

Our novel bandpass filter is a transconductance-capacitor (G_m–C) circuit that exhibits Q-peaking for small signals. A G_m–C circuit is normally operated within the linear range of all of the transconductance amplifiers. In our case, we deliberately employ nonlinearity in one of the amplifiers in order to evoke the cochlea's compressive behavior. The transconductance

[2]We define a transconductance function as one whose arguments are in units of Volts, and that is itself in units of Amperes. By contrast, a *transconductance gain*, with units of ampere/volts, is the derivative of the transconductance function with respect to input voltage. Further, the *small-signal transconductance gain* is the constant term of the transconductance gain.

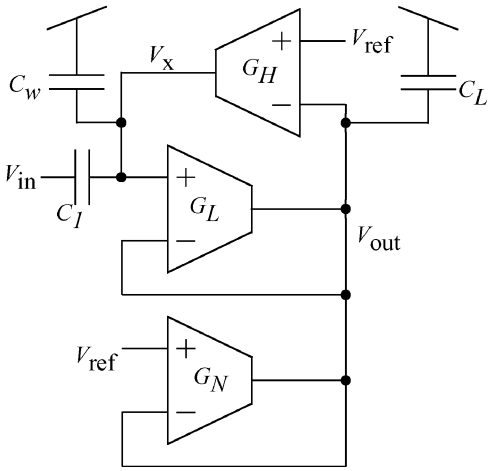

Fig. 3. Bandpass filter with adaptive quality factor. For fixed capacitor sizes, the center frequency and quality factor are determined by the geometric mean and ratio, respectively, of the G_H and G_L gains. The G_N transconductor augments the negative feedback action of the G_L element. If the transconductance gain of the G_N transconductor increases proportionally with the amplitude of $V_{\rm out}$, then the amount of damping in the circuit will also increase.

gain[2] of the nonlinear amplifier increases with input amplitude. Our filter is designed so that its damping coefficient is directly controlled by the nonlinear amplifier's transconductance gain. As such, the amount of Q-peaking reduces with increasing input amplitude.

The bandpass filter is based on the circuit of Fig. 3. It has a first-order roll off at a center frequency of

$$w_0 = \sqrt{\frac{G_H G_L}{C_L(C_1 + C_{\rm w})}} \tag{2}$$

while the quality-factor is nominally

$$Q = \sqrt{\frac{C_L G_H}{(C_1 + C_{\rm w})G_L}} \left(\frac{1}{1 + G_N/G_L}\right) \tag{3}$$

and the center frequency gain is

$$A_{w0} = C_1/(C_1 + C_{\rm w}). \tag{4}$$

C_1, $C_{\rm w}$, C_L are drawn capacitances and G_H, G_L, G_N are transconductance gains.

The G_m elements labelled G_H and G_L are linear, meaning that they have a constant transconductance gain. The G_N element, on the other hand, has a level-dependent transconductance gain, which is of the general form

$$G_N = f(\widetilde{V}_{\rm out}) \tag{5}$$

where $\widetilde{V}_{\rm out}$ is the energy of $V_{\rm out}$, and $f(\cdot)$ is a symmetric monotonically-increasing function. Substituting (5) into (3), we see that the quality factor is not constant, but is dependent on $\widetilde{V}_{\rm out}$. Specifically, Q decreases with increasing levels of $\widetilde{V}_{\rm out}$. The simplest form of $f(\cdot)$ is a quadratic function of $V_{\rm out}$, which would represent the instantaneous energy of the output voltage. In our design, the nonconstant transconductance gain is

$$G_N = N\left(1 + \alpha(V_{\rm out})^2/U_{\rm T}^2\right) \tag{6}$$

where N is some programable constant, $U_{\rm T}$ is the thermal voltage, and α is a coefficient to be determined.

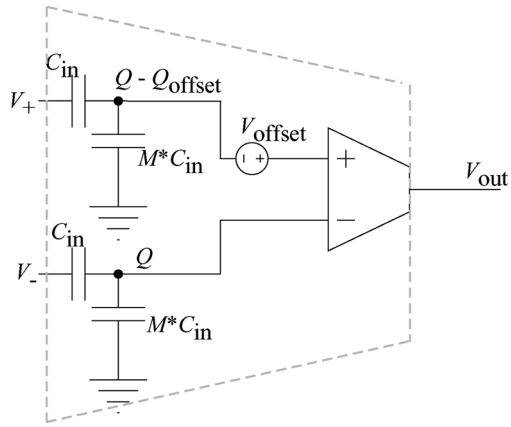

Fig. 4. Highly linear OTA. The inputs to a simple OTA are attenuated via capacitive division. Injection and tunnelling (through tunnelling capacitors, not shown) are used to precisely control the amount of charge on the floating nodes.

IV. Transconductance Elements

A. Low-Distortion Operational Transconductance Amplifier

The G_H and G_L elements are highly linear, meaning that they exhibit low distortion over a wide range of input voltages. We based their design on the simple, nine-transistor current mirror operational transconductance amplifier (OTA) [18].

There are three major sources of distortion from a simple OTA [19]. The first is large differential inputs to the differential pair, which cause the amplifier's transconductance gain to vary widely. The second source of distortion is finite offset due to device mismatch, which introduces even-order harmonics. Finally, an inappropriate input common-mode voltage may push either of the differential-pair transistors or the tail transistor out of saturation. We deal with all three sources of distortion by employing capacitive attenuation at the differential-pair inputs, as shown in Fig. 4.

The OTA input is attenuated by a factor of $M + 1$ before being applied to the differential pair. A large value of M ensures that the differential-pair input will never vary enough to alter the transconductance gain significantly.

The input nodes of the differential pair have no dc path to ground, meaning that, under normal operating conditions, any charge stored on them is nonvolatile. However, we can use the high-field phenomena of hot-electron injection and Fowler–Nordheim tunneling to change the amount of charge that is stored on these nodes [20]. In particular, we can modify the amount of stored charge so as to compensate for the amplifier's offset. Consider an input offset of $V_{\rm offset}$ and a difference in charge on the differential-pair input nodes of $Q_{\rm offset}$, as shown in Fig. 4. We set the difference in charge to satisfy

$$Q_{\rm offset} = V_{\rm offset} C_{\rm in}(M + 1) \tag{7}$$

which effectively removes the offset.

From Fig. 4, the common-mode input voltage, $V'_{\rm cm}$ of the differential pair is

$$V'_{\rm cm} = \frac{Q}{C_{\rm in}(M + 1)} + \frac{V_{\rm cm}}{M + 1}. \tag{8}$$

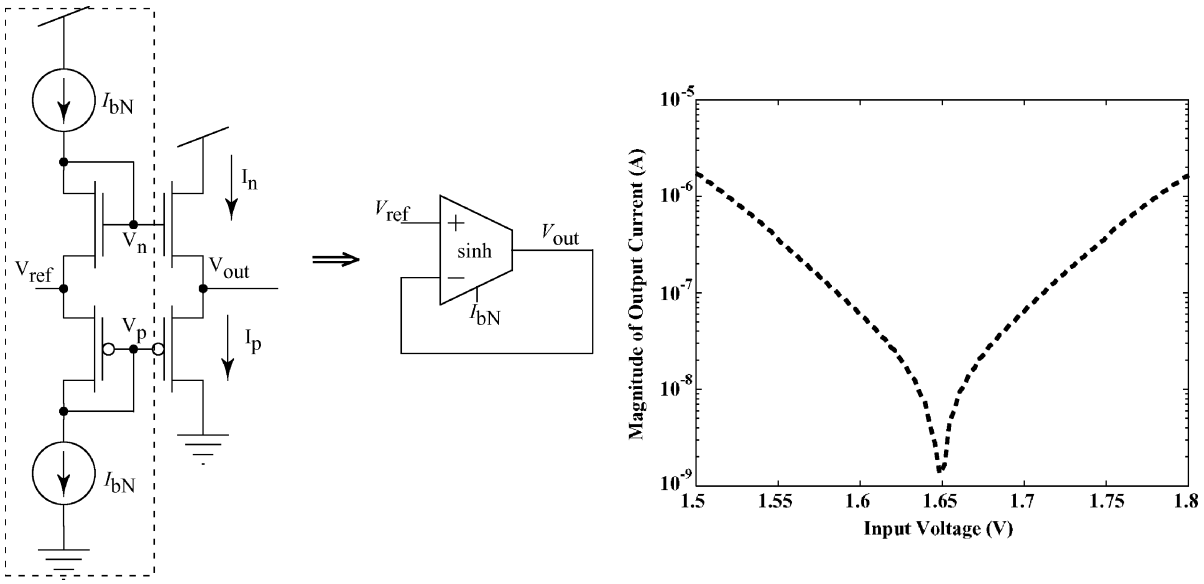

(a) (b)

Fig. 5. Nonlinear transconductance element. (a) Circuit implementation. $V_{\rm n}$ and $V_{\rm p}$ are fixed voltages that are set by the bias circuitry shown in the dashed box. The output node is $V_{\rm out}$. The output current is $I_{\rm n} - I_{\rm p}$. (b) Experimental current-voltage curve. When the $V_{\rm out}$ voltage is swept, the magnitude of the output current displays a logarithmic trend for large values of $V_{\rm out} - V_{\rm ref}$, which is characteristic of the sinh function.

We adjust the value of Q to ensure that the differential-pair and tail transistors are always in saturation.

Employing injection and tunneling the way we do precludes the need for a high-impedance-based biasing scheme, which would actually increase distortion at the low frequencies [21]. As we show in the experimental results section, our precise control of the floating-node charges results in a significant lowering of distortion.

B. Nonlinear Transconductance Element

The gain of (6) is provided by a transconductance element with the following nonlinear transfer function

$$I_{GN} = N\left(V_{\rm out} + \alpha (V_{\rm out})^3 / 3U_{\rm T}^2\right) \tag{9}$$

which we implemented with the circuit shown in Fig. 5(a). For the purpose of analysis, we will assume that the transistors in this circuit are operated in subthreshold. The circuit's behavior is similar for above-threshold operation, but its analysis would require a more complex transistor model that is valid in all regions of operation. So, assuming that the bias voltages $V_{\rm n}$ and $V_{\rm p}$ ensure subthreshold operation, the nMOS and pMOS drain currents are, respectively

$$I_{\rm n} = I_1 e^{\kappa_n V_{\rm n}/U_{\rm T}} e^{-V_{\rm out}/U_{\rm T}} \tag{10}$$

$$I_{\rm p} = I_2 e^{-\kappa_p V_{\rm p}/U_{\rm T}} e^{V_{\rm out}/U_{\rm T}} \tag{11}$$

where $I_{1,2}$ are pre-exponential current terms that depend largely on device dimensions and doping concentrations, and $\kappa_{n,p}$ are the body-effect coefficients.

Defining $V_{\rm ref}$ and $I_{\rm bN}$ as

$$V_{\rm ref} = \left(U_{\rm T} \log(I_1/I_2) + (\kappa_n V_{\rm n} + \kappa_p V_{\rm p})\right)/2 \tag{12}$$

$$I_{\rm bN} = 2\sqrt{I_1 I_2} e^{(\kappa_n V_{\rm n} - \kappa_p V_{\rm p})/U_{\rm T}} \tag{13}$$

we can write the output as

$$\begin{aligned} I_{\rm n} - I_{\rm p} &= I_{\rm bN}\left(e^{(V_{\rm ref}-V_{\rm out})/U_{\rm T}} - e^{(V_{\rm out}-V_{\rm ref})/U_{\rm T}}\right)/2 \\ &= -I_{\rm bN}\sinh\left((V_{\rm out}-V_{\rm ref})/U_{\rm T}\right) \\ &\approx \frac{-I_{\rm bN}}{U_{\rm T}}\left((V_{\rm out}-V_{\rm ref}) + (V_{\rm out}-V_{\rm ref})^3/6U_{\rm T}^2\right) \end{aligned} \tag{14}$$

which is equivalent to (9) if we associate $-I_{\rm bN}/U_{\rm T}$ with N, set $\alpha = 1/2$ and define $V_{\rm ref}$ as the reference voltage. Notice that (14) resembles the transfer function of a transconductance amplifier with inputs $V_{\rm out}$, $V_{\rm ref}$ and a bias current of $I_{\rm bN}$. We therefore model the nonlinear transconductor as an amplifier in negative feedback, as shown in Figs. 3 and 5(a).

V. Circuit Analysis

Since our filter involves an explicit nonlinearity, the classical small-signal paradigm is inadequate for performing any rigorous analysis. Instead, we employ tools from nonlinear dynamical systems theory to understand its behavior.

A. Quality Factor Adaptation

Applying Kirchhoff's current law (KCL) to both nodes of Fig. 3, we write

$$\begin{aligned} C_L\frac{dV_{\rm out}}{dt} &= G_L(V_{\rm x} - V_{\rm out}) - I_{\rm bN}\sinh\left(\frac{V_{\rm out}}{U_{\rm T}}\right) \\ (C_1 + C_{\rm W})\frac{dV_{\rm x}}{dt} &= -G_H V_{\rm out} + C_1\frac{dV_{\rm in}}{dt} \end{aligned} \tag{15}$$

where we have assumed subthreshold operation of the nonlinear conductance and all of the voltages are referenced to $V_{\rm ref}$. As a single second-order equation, (15) can be written as

$$\begin{aligned} \frac{C_L C_{\rm T}}{G_H G_L}\frac{d^2V_{\rm out}}{dt^2} &= -V_{\rm out} - \frac{C_1}{G_H}\frac{dV_{\rm in}}{dt} \\ &\quad - \frac{C_{\rm T}}{G_H}\frac{dV_{\rm out}}{dt}\left(1 + \frac{I_{\rm bN}}{U_{\rm T}G_L}\cosh\left(\frac{V_{\rm out}}{U_{\rm T}}\right)\right) \end{aligned} \tag{16}$$

where $C_{\mathrm{T}} = C_1 + C_{\mathrm{w}}$. The corresponding dimensionless form of (16) is

$$\ddot{y} = -H_1 L_1 y - L_1 \dot{y}\,(1 + c \cdot \cosh(y)) + L_1 \dot{u} \qquad (17)$$

where the variables x, y and u are related to the voltages V_{x}, V_{out} and V_{in}, respectively. H_1 and L_1 are proportional to G_H and G_L respectively, while c is equal to $I_{\mathrm{bN}}/(U_{\mathrm{T}} G_L)$. Note that c is the ratio of the small-signal transconductance gains of the G_N and G_L amplifiers.

To further simplify the analysis, we normalize (17) by setting its natural frequency, $\sqrt{H_1 L_1}$, to one. Then, we study the filter's response to a pure-tone input of unit frequency. Equation (17) is now

$$\ddot{y} + y = -L_1\,(\dot{y}\,(1 + c \cdot \cosh(y)) + F\cos(\tau)) \qquad (18)$$

where the input amplitude is F.

Notice that the nominal value of Q—that is, without the effect of the nonlinearity—is equal to $1/L_1$. To enhance the sensitivity and frequency selectivity bandpass filter, it normally has a Q of 5 to 10. Accordingly L_1 is a small, perturbation parameter and (18) is simply a resonator of unit frequency (LHS) that is perturbed by some nonlinear damping and a forcing function (RHS).

Using Lindstedt's method for perturbation analysis [22], the solution to (18) is

$$y = A\cos(\tau) + \mathrm{O}(L_1) \qquad (19)$$

where A, the amplitude of the fundamental frequency, is given by the following implicit function

$$A\left(1 + c\left(1 + \frac{A^2}{8} + \frac{A^4}{192} + \frac{A^6}{9216}\right)\right) - F = 0 \qquad (20)$$

and $\mathrm{O}(L_1)$ are higher harmonics. For values of $A < 2\sqrt{2/c}$, the filter's center frequency gain is approximately $1/(1+c)$. However, as the output signal amplitude increases, the center frequency gain reduces. The dimensionless quantity y is normalized as V/U_{T}. So, with a value of $U_{\mathrm{T}} = 25$ mV, $A = 2\sqrt{2/c}$ physically corresponds to an output voltage amplitude of $50\sqrt{2/c}$ mV. It is important to note that c is a ratio of transconductances. In VLSI circuits, physical ratios match much better than do absolute values, meaning that the compression characteristics of the filter ought to vary minimally across different chips. Fig. 6 shows plots of (20) for various values of $c = I_{\mathrm{bN}}/(U_{\mathrm{T}} G_L)$. Higher values of c cause the knee to occur at lower values of output voltage.

B. Harmonic Distortion

The sinh nonlinearity allows our filter's quality factor to adaptively reduce with increasing output amplitude, as desired. Unfortunately, the nonlinearity also introduces harmonic distortion, which is embodied in the $\mathrm{O}(L_1)$ term of (19).

We arrive at an estimate of the distortion by solving (18) for higher order perturbation methods. The approximate total harmonic distortion (THD) is

$$\mathrm{THD}(\%) = cL_1 \frac{A^2}{64}\left(1 + \frac{A^2}{16} + \frac{A^4}{640}\right) \cdot 100. \qquad (21)$$

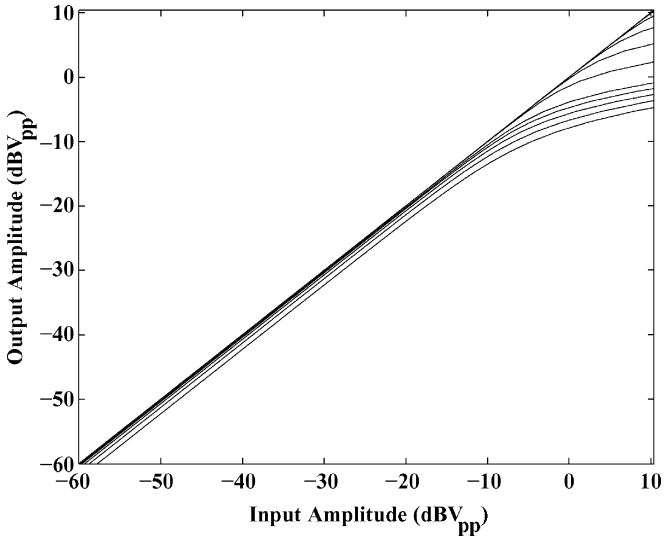

Fig. 6. Theoretical knee control. Larger values of $c = I_{\mathrm{bN}}/(U_{\mathrm{T}} G_L)$ elicit lower knee values. The four curves with the most compression shown are for $c = 0.046$, 0.086, 0.16, and 0.3.

As (21) suggests, we can reduce the amount of distortion, independently of the amount of compression, by reducing the value of L_1. Recall that the filter's nominal quality factor is $1/L_1$. So, reducing distortion by keeping L_1 small is not at odds with the desire to achieve high sensitivity and frequency selectivity. The fact that the distortion is reducible without affecting the amount of compression is crucial to distinguishing this filter's adaptive behavior from the effects of unwanted, so-called instantaneous nonlinearity in other circuits.

C. Noise

The filter's distortion characteristics determine its largest permissible input. In this section, we analyze its noise performance, so as to define the smallest useful signal. We model noise in the filter by placing a noise source at the input of each of the otherwise noise-free amplifiers, as shown in Fig. 7. The total noise output power is given as

$$\begin{aligned}\bar{n}^2_{\mathrm{out}} = &\int_0^\infty \frac{n_H^2}{\left(1 - \omega^2 \frac{C_L C_{\mathrm{T}}}{G_H G_L}\right)^2 + \omega^2 \frac{C_{\mathrm{T}}^2}{G_H^2}} d\omega \\ &+ \int_0^\infty \frac{n_L^2 \omega^2 \frac{C_{\mathrm{T}}^2}{G_H^2}}{\left(1 - \omega^2 \frac{C_L C_{\mathrm{T}}}{G_H G_L}\right)^2 + \omega^2 \frac{C_{\mathrm{T}}^2}{G_H^2}} d\omega \\ &+ \int_0^\infty \frac{n_N^2 \omega^2 \frac{C_{\mathrm{T}}^2 G_N^2}{G_H^2 G_L^2}}{\left(1 - \omega^2 \frac{C_L C_{\mathrm{T}}}{G_H G_L}\right)^2 + \omega^2 \frac{C_{\mathrm{T}}^2}{G_H^2}} d\omega \end{aligned} \qquad (22)$$

where $n^2_{H,L,N}$ are noise power densities and G_N has been assumed to be a constant that is much less than G_L. If the circuit's flicker noise is negligible compared to thermal noise, then $n^2_{H,L,N}$ are independent of frequency. In this case the integrals of (22) can be evaluated to give

$$\bar{n}^2_{\mathrm{out}} = n_H^2 \frac{\pi G_H}{2C_{\mathrm{T}}} + n_L^2 \frac{\pi G_L}{2C_L} + n_N^2 \frac{\pi G_N^2}{2C_L G_L}. \qquad (23)$$

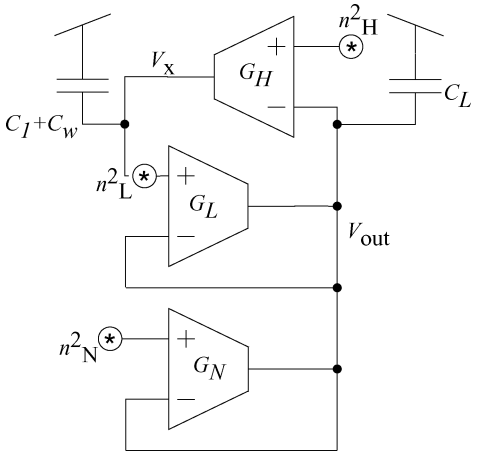

Fig. 7. Schematic for analyzing noise in filter.

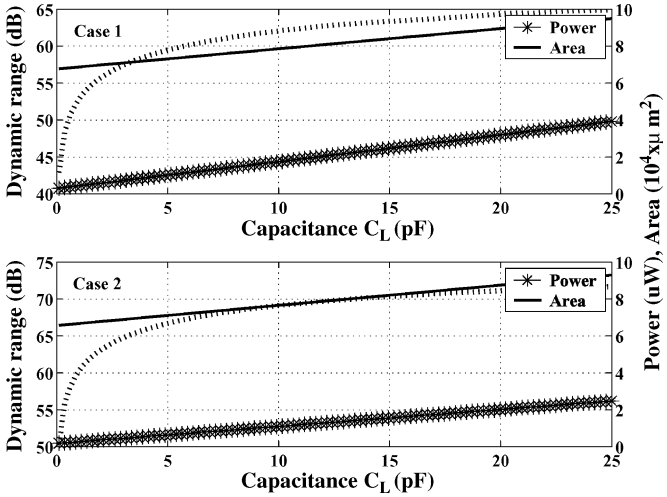

Fig. 8. Tradeoff between dynamic range (dashed line, left horizontal axis), area (solid line, right axis) and power (asterisks, right axis) with C_L size. All three specifications—dynamic range, power and area—increase with increasing values of C_L, but the different design parameters of case 1 versus case 2 yield different performance specifications. Capacitor values for the upper panel (case 1) are $C_1 = 2$ pF, $C_w = 2.9$ pF, and $M_H = 10$, $M_L = 100$. In the lower panel (case 2), we set $C_1 = 3$ pF, $C_w = 0.1$ pF, keeping the other variables the same. Dynamic range is calculated using (29) and assuming a rail-to-rail linear range of 3.3 V. Power consumption is calculated using (2) and (3) for $Q = 2$ at a center frequency of 1 kHz.

For a given bias current, subthreshold transistors yield the highest possible transconductance. For this reason, we will assume that the OTAs are operated in the subthreshold regime. The input-referred thermal noise density of a subthreshold OTA is

$$n^2 = \frac{2KqU_{\mathrm{T}}^2}{\kappa^2 I_{\mathrm{b}}\pi} \tag{24}$$

where K is the effective number of noise-contributing transistors, q is the charge of one electron and I_{b} is the amplifier's bias current [23]. K is approximately equal to 8 in our OTA [18]. For an OTA with an input capacitive attenuation factor $(M+1)$, the bias current must be multiplied by $(M+1)$ to maintain the transconductance gain and bandwidth. Further, the noise density referred to the input of the capacitive divider is the original OTA input-referred noise density multiplied by $(M+1)^2$. So, the input-referred noise densities of G_H and G_L are

$$\begin{aligned} n_H^2 &= (M_H+1)^2 \frac{2KqU_{\mathrm{T}}^2}{\kappa^2(M_H+1)I_{\mathrm{bH}}\pi} \\ &= (M_H+1)\frac{2KqU_{\mathrm{T}}^2}{\kappa^2 I_{\mathrm{bH}}\pi} \end{aligned} \tag{25}$$

$$n_L^2 = (M_L+1)\frac{2KqU_{\mathrm{T}}^2}{\kappa^2 I_{\mathrm{bL}}\pi}, \tag{26}$$

where $(M_{H,L}+1)$ are the capacitive attenuation factors of amplifiers G_H and G_L. The noise density of G_N is

$$n_N^2 = \frac{qU_{\mathrm{T}}^2}{\kappa^2 I_{\mathrm{bN}} 2\pi}. \tag{27}$$

We are assuming in this analysis that all of the body-effect coefficients are equal to κ. Using the fact that $G_H = \kappa I_{\mathrm{bH}}/2U_{\mathrm{T}}$, $G_L = \kappa I_{\mathrm{bL}}/2U_{\mathrm{T}}$ and $G_N = \kappa I_{\mathrm{bN}}/U_{\mathrm{T}}$, we substitute (25), (26), and (27) into (23) to get

$$\begin{aligned} \bar{n}_{\mathrm{out}}^2 &= \frac{KqU_{\mathrm{T}}}{4\kappa C_{\mathrm{T}}}\left(M_H+1+\frac{C_{\mathrm{T}}}{C_L}\left(M_L+1+\frac{2I_{\mathrm{bN}}}{KI_{\mathrm{bL}}}\right)\right) \\ &\approx \frac{KqU_{\mathrm{T}}}{4\kappa C_{\mathrm{T}}}\left(M_H+1+\frac{C_{\mathrm{T}}}{C_L}(M_L+1)\right). \end{aligned} \tag{28}$$

From (4), the total input-referred noise at the center frequency is

$$\bar{n}_{\mathrm{in}}^2 \approx \frac{C_{\mathrm{T}}}{C_1}\frac{KqU_{\mathrm{T}}}{4C_1\kappa}\left(M_H+1+\frac{C_{\mathrm{T}}}{C_L}(M_L+1)\right). \tag{29}$$

We can minimize the noise, and hence maximize the dynamic range, by ensuring $C_L \gg C_1 \gg C_w$. Such a tactic comes at the expense of a larger circuit area and increased power consumption. Fig. 8 illustrates the tradeoffs involved.

D. Stability

Simple eigenvalue analysis reveals that the circuit described by (17), is a small-signal stable system. However, as previous hearing-application front ends have shown, it may be possible for the filter's nonlinearity to cause large-signal instability [24]. This concern is particularly relevant in our case, given that we are explicitly introducing and exploiting a nonlinear function in our design.

A complete analysis of large-signal stability must regard all of the G_m elements in Fig. 3 as nonlinear; despite our best efforts, G_H and G_L can never be perfectly linear. So, instead of the constant gains H_1 and L_1, we represent the transconductances of G_H and G_L as H and L, respectively. H and L are nonlinear functions of their respective input voltages with the following properties. First of all, they are monotonically-increasing functions, which means that larger and larger inputs will elicit larger and larger outputs. Secondly, they pass through the origin, that is $H(0) = L(0) = 0$. In practice, H and L are sigmoidal functions as they are formed from a differential pair. We write the filter's describing equations as

$$\begin{aligned} \frac{dy}{d\tau} &= L(x-y) - c\cdot L\sinh(y) \\ \frac{dx}{d\tau} &= -H(y) + \frac{du}{d\tau}. \end{aligned} \tag{30}$$

To prove large-signal stability in a dynamical system, it is sufficient to identify its fixed point, and to prove that the system always tends towards this point, regardless of initial conditions, and independent of any linearizing approximations. Setting

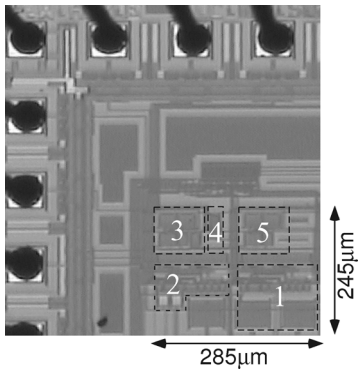

Fig. 9. Die photograph of the bandpass filter. The portions labelled 1–5 are, respectively, the G_L amplifier, the G_H amplifier, the output buffer for the $V_{\rm out}$ node, the sinh transconductor, and the output buffer for the $V_{\rm x}$ node. The integrating capacitors $C_{\rm w}$, C_L and C_1 are not labelled, but they are included in the $285 \times 245\ \mu{\rm m}^2$ area shown here.

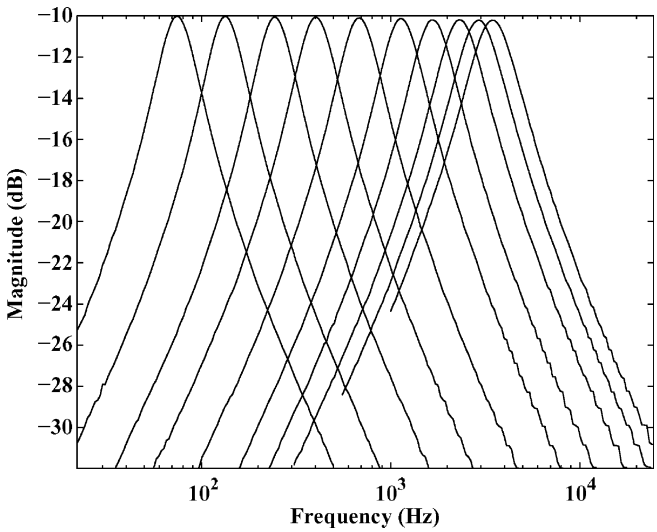

Fig. 10. Center frequency control. The bandpass filter center frequency is directly proportional to the geometric mean of the gains G_L and G_H, and is tunable independent of the automatic gain control action.

all the time derivatives in (30) to zero, and from the property $H(0) = L(0) = 0$, we identify the origin as the system's unique fixed point.[3] Now, we define an energy-like function

$$V(y,e) = \int_0^y H(\chi) + \sinh(\chi) d\chi + \int_0^e L(\zeta) d\zeta \qquad (31)$$

where $e = x - y$.

From the monotonicity of H, L and sinh, notice that the value of $V(y,e)$ is positive everywhere except at the origin, where it is equal to zero. Thus, the energy-like function is minimized at the origin. Further, the time derivative of $V(y,e)$ is negative everywhere but at the origin, where it is equal to zero. So, whenever it is not at the origin, the system possesses some positive amount of $V(y,e)$, which it dissipates over time. When $V(y,e) = 0$, the dissipation ceases, at which point the state variables are now at the origin. This argument shows, as would a more formal application of Lyapunov's Theorem [25], that the circuit is large-signal stable.

VI. Circuit Implementation and Experimental Results

We fabricated a prototype of the adaptive-Q bandpass filter in a 0.5-μm process available from MOSIS, Fig. 9. The pMOS transistors of amplifiers G_H and G_L were sized 30 μm/3 μm to allow for large subthreshold currents. The nMOS transistors in both amplifiers were sized at 15 μm/3 μm. The nMOS and pMOS transistors of the G_N element were sized at 3 μm/1.5 μm and 6 μm/1.5 μm, respectively. The G_N transistors were sized relatively small to facilitate the tuning of small values of $I_{\rm bN}$, which would correspond to small values of c (for testing purposes, $V_{\rm n}$ and $V_{\rm p}$ of Fig. 5(a) were not set by bias circuitry, but by an off-chip DAC.). The drawn capacitor values were $C_1 = C_L = 2$ pF, $C_{\rm w} = 2.9$ pF.[4] Since $V_{\rm out}$ is an attenuated version of the input and experiences compression at that, we chose $(M_H + 1) = 11$ for the capacitive divider ratio of G_H. The positive input of G_N is $V_{\rm x}$, which has voltage excursions that can approach the power rails. The capacitive divider ratio for G_L was therefore chosen to be $(M_L + 1) = 101$. Our design choices placed the prototype filter in the Case 1 of Fig. 8. With $C_L = 2$ pF, the circuit area is 6.9e4 μm^2. The predicted dynamic range and power consumption are 55.8 dB and 0.6 μW (for $Q = 2$ at a 1-kHz center frequency), respectively.

As the results of Fig. 10 show, the circuit behaves as a second-order bandpass filter as expected, and has a tunable center frequency across the audio range. When programmed to a center frequency of 1.18 kHz and a Q of 2, the bandpass filter consumes 1.32 μW of power, which is twice the amount predicted in Fig. 8. Power consumption is directly proportional to the filter's center frequency. For instance, if the filter were programmed to a center frequency of 11.8 kHz, it would consume 13.2 μW.

Experimental measurements confirm that our filter exhibits the adaptive behavior that we designed for. Fig. 11 shows how the magnitude-frequency response of the filter changes with different input amplitudes. For input amplitudes less than 5.6 $\rm mV_{pp}$, the center frequency gain is almost -10 dB. The gain reduces progressively for larger input amplitudes and drops by over 10 dB when the input amplitude exceeds 2 $\rm V_{pp}$.

Fig. 12 demonstrates experimental control of the threshold knee point. The various curves correspond to different values of $I_{\rm bN}$, with fixed G_L. We set $I_{\rm bN}$ with the voltages $V_{\rm p}$ and $V_{\rm n}$. For $V_{\rm p} = 3.3$ V and $V_{\rm n} = 0$ V, $I_{\rm bN}$ is essentially zero, meaning that compression is turned off. For nonzero values of $I_{\rm bN}$, compression is observed at different output amplitude knee points. It was difficult to achieve fine resolutions for small values of $I_{\rm bN}$,

[3]The property that $H(0) = L(0) = 0$ is simply for the convenience of defining the fixed point at the origin. The point $(x,y) = (0,0)$ in state space corresponds to the physical voltages $V_{\rm x}$ and $V_{\rm out}$ being equal to $V_{\rm ref}$, plus some offset. That is, the operating point of $V_{\rm x}$ is $V_{\rm ref}$ plus the offset of the G_H element, while the operating point of $V_{\rm out}$ is $V_{\rm ref}$ plus the sum of the offsets of G_H and G_L.

[4]Our analysis shows that these are not the optimal values for a low-noise filter. For this prototype circuit, we were more concerned with demonstrating low-power, low-distortion gain adaptation than in optimizing for noise performance.

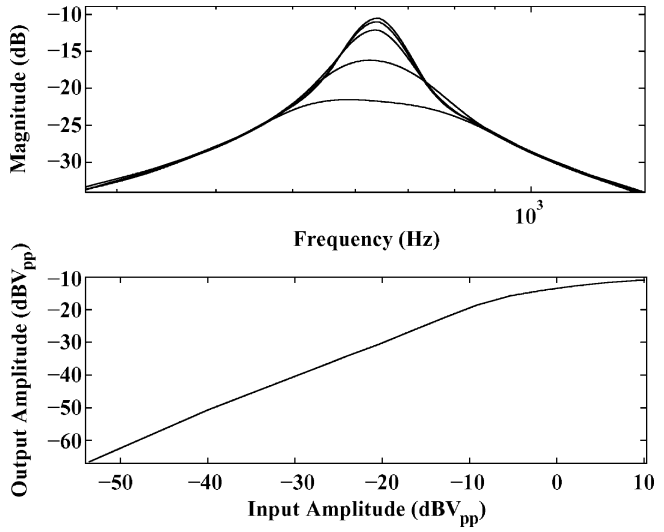

Fig. 11. Quality factor adaptation. The upper panel depicts a reduction in Q from 8 to 2 with increasing input amplitudes. The transfer curves shown are for the following input amplitudes: -5.2 dBV$_{\rm pp}$, -4.4 dBV$_{\rm pp}$, -2.3 dBV$_{\rm pp}$, 4 dBV$_{\rm pp}$, 10.3 dBV$_{\rm pp}$. The bottom panel shows the same information as a plot of output amplitude versus input amplitude at the filter's center frequency. The filter was programmed to a center frequency of 1.18 kHz and $Q = 10$.

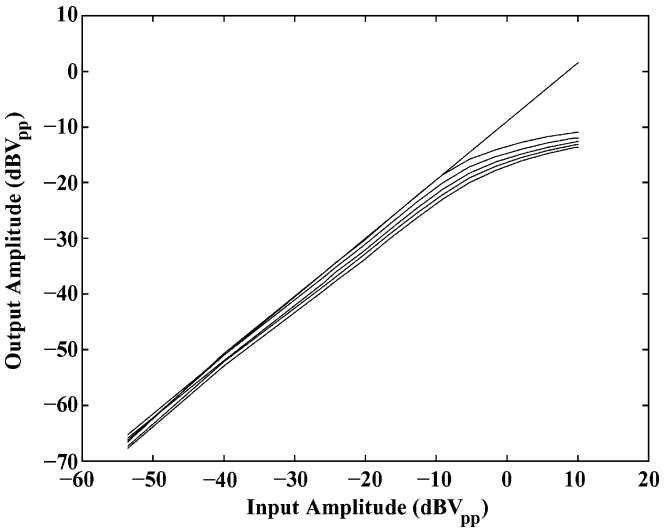

Fig. 12. Threshold knee point control. The normalized input-output amplitude response, measured at the center frequency, shows that the gain exhibits compressive behavior past a certain output amplitude threshold. This threshold point can be adjusted by varying the transconductance gain of the sinh element (effectively by varying its bias current).

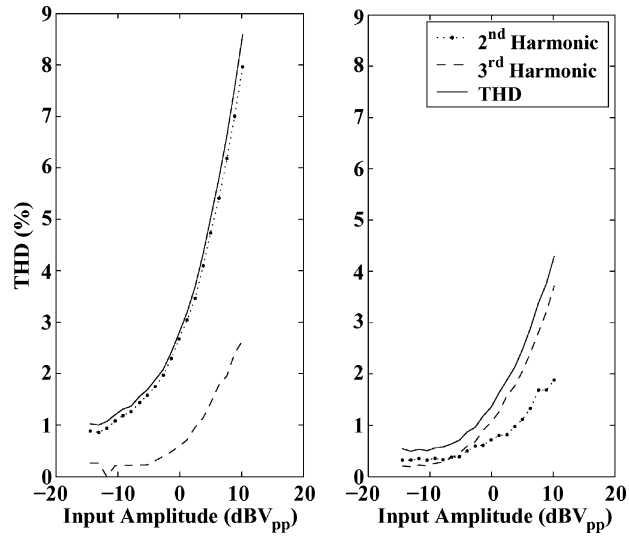

Fig. 13. THD reduction with offset removal. The left panel shows the distortion numbers for when an equal amount of charge is placed (via injection and tunnelling) on the floating gates of each differential-pair in the filter. Transistor mismatch causes offset, which is observed as a large second harmonic. When the offset is compensated for with an uneven amount of charge, the second harmonic reduces, as shown in the right-hand panel. Offset removal should ordinarily not affect odd-order harmonics, and the slight increase in third harmonic content is due to measurement error.

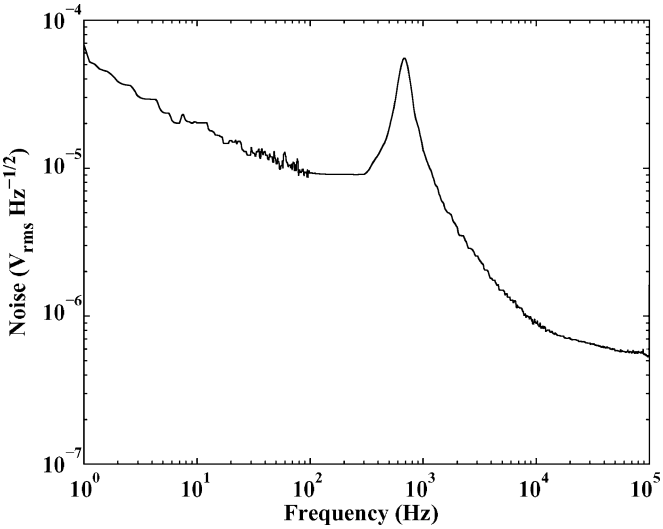

Fig. 14. Measured noise power spectrum. The output noise has a bandpass profile (from G_L and G_N) summed with a lowpass profile (from G_H). The flicker noise corner frequency is 100 Hz, which is just low enough for thermal noise to dominate.

which is why the curves shown in Fig. 12 all have knee-points for output amplitudes close to -20 dB.

Our explicit use of nonlinearity raises the question of how much distortion our circuit will suffer. Fig. 13 supports our claim that the amount of distortion is minimal. The sinh nonlinearity contributes most of the third harmonic, since the other two G_m elements have been linearized via capacitive attenuation. However, there is a significant second harmonic in the left panel of Fig. 13, due to input offset in the G_H and G_L amplifiers. By adjusting the amount of charge stored on their differential-pair input gates, we were able to reduce the offset significantly. This improvement is shown in the right panel of Fig. 13, where the second harmonic has fallen from a maximum of 8% to less than 2%. At the maximum input amplitude, the THD for the improved case is 4.3%. This THD figure falls within the acceptable range for cochlear implants [21]. Some subjective tests of hearing aids have suggested that wearers do not find THDs of 3 to 6% disagreeable [26]. Still, we acknowledge that our THD figure is on the high side for hearing aids, given that current models exhibit THDs of 1% to 3%.

The measured output noise power spectrum is shown in Fig. 14. The total integrated input-referred noise is 2.2 mV$_{\rm rms}$,

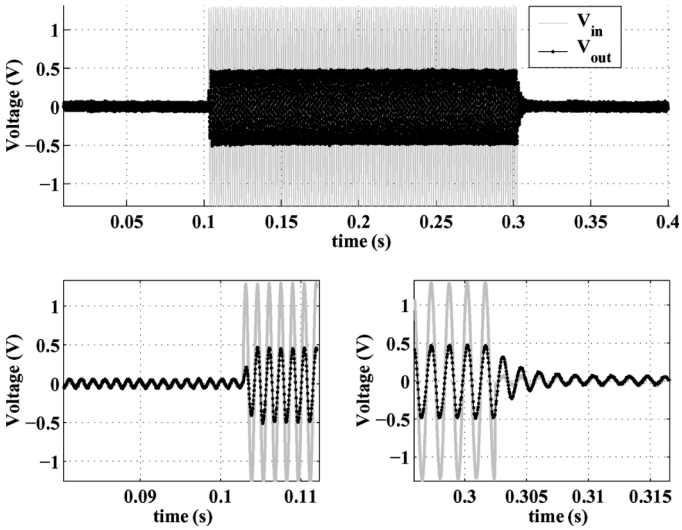

Fig. 15. Filter response to input bursts. As the zoomed-in figures show, the attack and release time of the gain control scheme correspond to about one period of the input signal.

which gives an input dynamic range of 54.5 dB, a close match to the theoretical value of Fig. 8.

Designers quantify the adaptation speed of conventional AGCs with the attack and release times [4]. In our case, since the bandpass filter incorporates the AGC action, the time constant of the input signal is always well-defined. (It is roughly the reciprocal of the filter's center frequency.) It therefore makes sense to employ adaptation speeds that are on the same order of the expected input-signal time constant, as shown in Fig. 15. Also, noise-pumping is not a concern for the following reasons. First, our filter's gain adapts smoothly with input amplitude. Secondly, the adaptation is largely restricted to a narrow band around the center frequency, which ensures that the gain applied to noise of a given level is always constant, and not influenced by other noise signals that are outside the bandwidth of interest.

VII. Discussion of Results

The experimental results of our prototype circuit conform to our theoretical claims. However, a practical hearing aid would require more particular specifications.

Consider designing a hearing aid for patients with mild to severe hearing loss. While this application requires compression of up to 40 dB, our prototype circuit only exhibits a maximum of 15 dB. One solution is to cascade two filters per channel, in order to create a fourth-order bandpass filter, which would provide 30 dB of compression. The cost of this approach is a doubling in area and power consumption. Also, the dynamic range of the filter is reduced by A_{w0}. We can get the remaining 10 dB of compression from a wide-band automatic gain control. The hearing aid still offers multichannel compression, provided the patient experiences at least a 10-dB hearing loss across all frequency bands.

Microphones deliver up to 80 dB of output signal range [27]. So, even assuming that the signal is compressed by 10 dB, our bandpass filter still has to support a 70-dB dynamic range of input. Our prototype circuit does not meet this specification but

TABLE I
Comparison of Filter Performance to Other Work

	This work	[21]	[28]	[29]
Dynamic range (dB)	55	62	57	62
THD (%)	4.3	5	2	1.1
Power (μW)	1.12	2	6	16
Compression (dB)	15	0	0	0

Fig. 8 suggests a design that would. If we chose $C_1 = 3$ pF, $C_{\rm w} = 0.1$ pF and $C_L = 10$ pF, then, at the expense of power and area, the filter would achieve a 70-dB dynamic range. Table I summarizes our filter's performance, in comparison to other filters that were designed for hearing instruments. The columns labeled The power consumption is normalized to that of a filter with a 1-kHz center frequency.

VIII. Conclusion

In this paper, we have presented a bandpass filter with dynamic range, power consumption, and size specifications that are similar to that of state-of-the-art filters for hearing applications [21], [28], [29]. The major advantage of our design over these other filters is that it incorporates adaptive Q control. For the current implementation of our filter, the measured compression range did not exceed 15 dB, meaning that cascading might be necessary, as would a wide-band AGC, to compress the microphone's output signal. Still, the inherent gain adaptation of our filter allows for multichannel compression. It also reduces the performance requirements of the wide-band AGC, which implies lower complexity and power consumption in the overall hearing aid design. In other words, our bandpass filter enables more sophisticated analog signal processing, at a lower power and area cost, than do other designs.

References

[1] S. T. Neely and D. O. Kim, "A model for active elements in cochlear biomechanics," *J. Acoust. Soc. Amer.*, vol. 79, pp. 1472–1480, 1986.
[2] D. S. Lum and L. D. Braida, "DSP implementation of a real-time hearing loss simulator based on dynamic expansion," in *Modeling Sensorineural Hearing Loss*, W. Jesteadt, Ed. Mahwah, NJ: Lawrence Erlbaum Associates, 1997, ch. 7, pp. 113–130.
[3] J. B. Allen, "Derecruitment by multiband compression in hearing aids," in *Modeling Sensorineural Hearing Loss*, W. Jesteadt, Ed. Mahwah, NJ: Lawrence Erlbaum Associates, 1997, ch. 6, pp. 99–112.
[4] T. Fortune, "Amplifiers and circuit algorithms of contemporary hearing aids," in *Hearing Aids: Standards, Options, and Limitations*, M. Valente, Ed. New York: Thieme Medical, 1996, ch. 4, pp. 157–209.
[5] A. M. Engebretson, "Benefits of digital hearing aids," *IEEE Eng. Med. and Biol. Mag.*, vol. 13, no. 2, pp. 238–248, 1994.
[6] B. W. Edwards, "Signal processing techniques for a dsp hearing aid," in *Proc. ISCAS'98*, Monterey, CA, May 1998, vol. 6, pp. 586–589.
[7] D. M. Chabries, D. V. Anderson, T. G. Stockham, Jr., and R. W. Christiansen, "Application of a human auditory model to loudness perception and hearing compensation," in *Proc. ICASSP'95*, May 1995, vol. 5, pp. 3527–3530.
[8] E. Fragniere, A. van Schaik, and E. A. Vittoz, "Design of an analogue vlsi model of an active cochlea," *Anal. Integr. Circuits Syst.*, vol. 13, no. 1, pp. 19–35, 1997.
[9] B. S. Wilson, D. T. Lawson, J. M. Müller, R. S. Tyler, and J. Kiefer, "Cochlear implants: Some likely next steps," *Annu. Rev. Biomed. Eng.*, vol. 5, pp. 207–249, 2003.
[10] W. A. Serdijn, A. C. van der Woerd, J. Davidse, and A. H. M. van Roermund, "A low-voltage low-power fully-integratable automatic gain control for hearing instruments," *IEEE J. Solid-State Circuits*, vol. 29, no. 8, pp. 943–946, Aug. 1994.

[11] A. C. Neuman, M. H. Bakke, C. Mackersie, S. Hellman, and H. Levitt, "The effect of compression ratio and release time on the categorical rating of sound quality," *J. Acoust. Soc. Amer.*, vol. 103, no. 5, pt. 1, pp. 2273–2281, May 1998.
[12] D. V. Anderson, "Model Based Development of a Hearing Aid," M.S. thesis, Brigham Young University, Provo, UT, 1994.
[13] D. V. Anderson, R. W. Harris, and D. M. Chabries, "Evaluation of a hearing compensation algorithm," in *Proc. ICASSP'95*, May 1995, vol. 5, pp. 3531–3533.
[14] E. W. Yund and K. M. Buckles, "Multichannel compression hearing aids: Effect of number of channels on speech discrimination in noise," *J. Acoust. Soc. Amer.*, vol. 97, no. 2, pp. 1206–1223, Feb. 1995.
[15] J. J. Zwislocki, Y. M. Szymko, and L. Y. Hertig, "The cochlea is an automatic gain control system after all," in *Diversity in Auditory Mechanics*. Singapore: World Scientific, 1996.
[16] B. M. Johnstone, R. Patuzzi, and G. K. Yates, "Basilar membrane measurements and the travelling wave," *Hear. Res.*, vol. 22, pp. 147–153, 1986.
[17] P. Dallos, "The active cochlea," *J. Neurosci.*, vol. 12, no. 12, pp. 4575–4585, 1992.
[18] R. R. Harrison and C. Charles, "A low-power low-noise cmos amplifier for neural recording applications," *IEEE J. Solid-State Circuits*, vol. 38, no. 6, pp. 958–965, Jun. 2003.
[19] B. Razavi, *Design of Analog CMOS Integrated Circuits*. New York: McGrawHill, 2001.
[20] P. Hasler, B. A. Minch, and C. Diorio, "Adaptive circuits using pfet floating-gate devices," in *Proc. Adv. Res. VLSI'99*, Atlanta, GA, Mar. 1999, pp. 215–229.
[21] C. D. Salthouse and R. Sarpeshkar, "A practical micropower programmable bandpass filter for use in bionic ears," *IEEE J. Solid-State Circuits*, vol. 38, no. 1, pp. 63–70, Jan. 2003.
[22] R. Rand, *Lecture Notes on Nonlinear Vibrations*. Ithaca, NY: The Internet-First University Press, 2003.
[23] R. Sarpeshkar, R. F. Lyon, and C. Mead, "A low-power wide-linear-range transconductance amplifier," *Anal. Integr. Circuits Syst.*, vol. 13, no. 1–2, pp. 123–151, 1997.
[24] R. F. Lyon and C. Mead, "An analog electronic cochlea," *IEEE Trans. Acoust., Speech, Signal Process.*, vol. 36, no. 7, pp. 1119–1134, Jul. 1988.
[25] H. K. Khalil, *Nonlinear Systems*. Upper Saddle River, NJ: Prentice-Hall, 2002.
[26] J. Agnew, "Hearing instrument distortion: What does it mean for the listener?," *Hea.r Instrum.*, vol. 39, no. 10, pp. 11–16, 1988.
[27] J. J. Neumann, Jr. and K. J. Gabriel, "A fully-integrated cmos-mems audio microphone," in *Proc. Int. Conf. Transducers, Solid-State Sensors, Actuat. and Microsyste.*, Jun. 2003, pp. 230–233.
[28] W. A. Serdijn, M. Broest, J. Mulder, A. C. Van Der Woerd, and A. H. M. Van Roermund, "A low-voltage ultra-low-power translinear integrator for audio filter applications," *IEEE J. Solid-State Circuits*, vol. 32, no. 4, pp. 577–581, Apr. 1997.
[29] L. Pylarinos and K. Pqhang, "Low-voltage programmable gm-c filter for hearing aids using dynamic gate biasing," in *Proc. ISCAS'05*, May 2005.

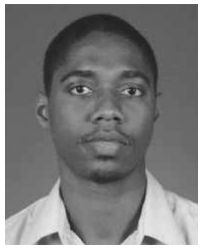

Kofi M. Odame (S'06) received the B.Sc. and M.Sc. degrees in electrical and computer engineering from Cornell University, Ithaca, NY, in 2002 and 2004, respectively. He is currently working toward the Ph.D. degree in the School of Electrical and Computer Engineering at Georgia Institute of Technology, Atlanta.

His research interest is in harnessing the inherent nonlinear characteristics of circuit devices to design cheap and efficient continuous-time processing systems.

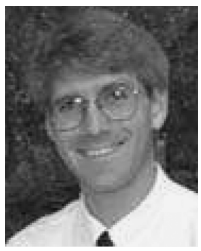

David V. Anderson (SM'05) received the B.S and M.S. degrees from Brigham Young University and the Ph.D. degree from Georgia Institute of Technology (Georgia Tech) in 1993, 1994, and 1999, respectively.

He is currently an Associate Professor in the School of Electrical and Computer Engineering, Georgia Tech, and co-director of CREST, the Center for Research in Embedded Systems Technology. His research interests include audio and psycho-acoustics, signal processing in the context of human auditory characteristics, and the real-time application of such techniques using both analog and digital hardware.

Dr. Anderson was awarded the National Science Foundation CAREER Award for excellence as a young educator and researcher in 2004 and the Presidential Early Career Award for Scientists and Engineers in the same year. He has over 100 technical publications and 7 patents/patents pending. Dr. Anderson is a senior member of the IEEE, and a member the Acoustical Society of America, American Society for Engineering Education, and Tau Beta Pi.

Paul Hasler (SM'02) received the B.S.E. and M.S. degrees in electrical engineering from Arizona State University, Tempe, in 1991, and the Ph.D. degree in computation and neural systems from California Institute of Technology, Pasadena, in 1997.

He is an Associate Professor in the School of Electrical and Computer Engineering, Georgia Institute of Technology, Atlanta. His current research interests include low power electronics, the use of floating-gate MOS transistors to build adaptive information processing systems, and "smart" interfaces for sensors.

Dr. Hasler received the National Science Foundation CAREER Award in 2001, and the Office of Naval Research YIP award in 2002. He received the Paul Raphorst Best Paper Award, IEEE Electron Devices Society, 1997, Best Student paper at CICC 2005, Best Sensors track paper, ISCAS 2005, a Best Paper Award at SCI 2001, and a Finalist for the Packard Young Investigator Award (1999).